Quantitative HAADF-STEM tomography of unsupported intermetallic Ga-Pd catalysts

2012 J. Phys.: Conf. Ser. 371 012024

(http://iopscience.iop.org/1742-6596/371/1/012024)

Quantitative HAADF-STEM tomography of unsupported intermetallic Ga-Pd catalysts

Rowan Leary[1], Zineb Saghi[1], Marc Armbrüster[2], Robert Schlögl[3], John Meurig Thomas[1] and Paul Midgley[1]

[1]Department of Materials Science and Metallurgy, University of Cambridge, Pembroke Street, Cambridge, CB2 3QZ, UK.
[2]Max-Planck-Institut für Chemische Physik fester Stoffe, Nöthnitzer Strasse 40, 01187 Dresden, Germany.
[3]Department of Inorganic Chemistry, Fritz Haber Institute of the Max Planck Society, Faradayweg 4-6, 14195 Berlin, Germany.

E-mail: rkl26@cam.ac.uk

Abstract. HAADF-STEM tomography has been used for characterisation of novel unsupported intermetallic Ga-Pd catalysts, with accompanying analysis by HRTEM and EDXS. Image processing techniques applied to the tomogram have facilitated segmentation and the subsequent extraction of size and shape parameters. The fidelity of the analysis has been critically examined, enabling identification of reconstruction artefacts and thereby more reliable determination of catalytically relevant properties. Further steps towards robust and accurate metrology by electron tomography are discussed.

1. Introduction

Ga-Pd intermetallic compounds have recently been shown to be highly stable and selective catalysts for the semihydrogenation of acetylene, where they outperform established systems [1]. This new class of catalyst has been realized by exploiting the covalent interactions in the well-ordered crystal structures of the intermetallic compounds, to stabilize isolated Pd sites on the catalyst surface. The stability of the Ga-Pd compounds under reaction conditions allows the direct relation of size, composition and morphology with catalytic properties and a knowledge-based development of new intermetallic catalysts. HAADF-STEM tomography has been undertaken for 3D characterization of unsupported Ga-Pd nanoparticle clusters (expected phase from XRD: $GaPd_2$) with particular interest in the size and shape of the particles, as well as their 3D arrangement with respect to one another. The 3D characterization has been complemented by HRTEM and EDXS for verification of phase and compositional homogeneity.

2. Experimental

HAADF-STEM tomography was performed on an FEI Tecnai F20 TEM operated at 200 kV, with a detector inner angle of ~45 mrad. The tilt-series was acquired in a semi-automated manner over a range of ±76° with a 2° tilt increment using FEI Xplore3D. The image series was aligned by cross-correlation and reconstruction performed using 40 iterations of the SIRT algorithm in FEI Inspect3D. Post-processing and visualisation were carried out using ImageJ and Avizo Fire. EDXS was also performed on the Tecnai F20 using an EDAX r-TEM ultra-thin window X-ray detector. For HRTEM a

JEOL 4000EX-II dedicated high-resolution microscope was operated at 400 kV. Phase identification was based on local Fourier transform (FT) analysis of the HRTEM images, with comparison to simulated diffraction patterns generated using CrystalMaker and SingleCrystal.

3. Results and discussion

3.1. HRTEM and EDXS

EDX point spectra shown in figure 1 suggest consistent composition, in keeping with the expected phase $GaPd_2$ [2]. The HRTEM data also supports the phase $GaPd_2$, and has been considered in some detail. The Ga-Pd phase diagram [2] shows a number of possible phases, which are known to have very similar lattice spacings and are therefore not easy to distinguish by FT analysis. Measured FTs from isolated particles have been carefully compared to simulated diffraction patterns for $GaPd_2$, using the recently refined structure parameters from Kovnir *et al.* [3] (orthorhombic, *Pnma* (no. 62), a = 5.4829(8) Å, b = 4.0560(4) Å, c = 7.7863(8) Å). An example supporting the suggested phase $GaPd_2$ is shown in figure 2a, and the crystallinity of smaller particles is confirmed by the diffractogram in figure 2b. While alternative phases could not be unequivocally ruled out in every case, simulated diffraction patterns for $GaPd_2$ were found to consistently fit all particles giving clear FTs with enough spots for reliable identification. The HRTEM images also show an amorphous layer around the particles, which is thought to be remnant organic from the synthesis process [4]. This may account for the oxygen peak in the EDX spectra.

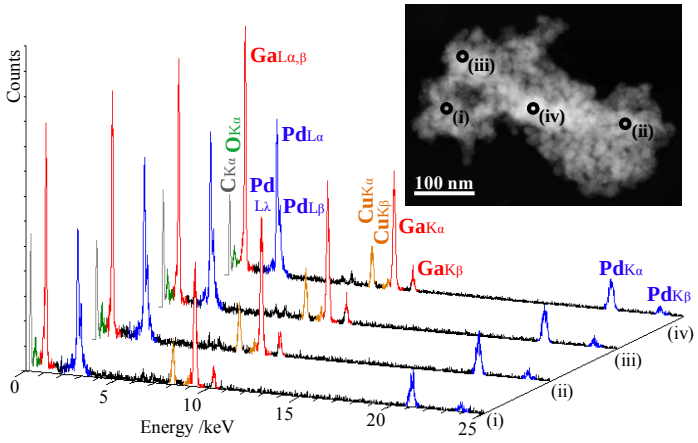

Figure 1. EDX point spectra. All spectra have been normalised to their GaL_α peak. (Colour online)

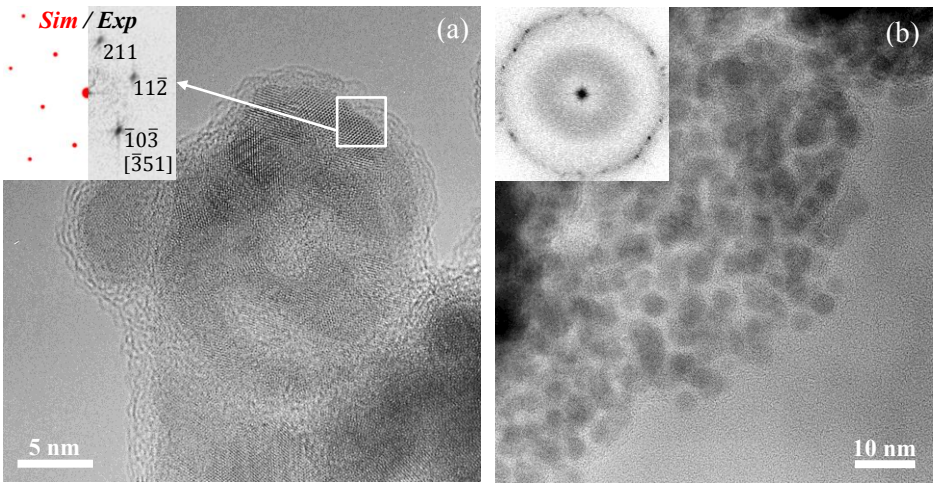

Figure 2. HRTEM images of (a) large and (b) smaller Ga-Pd particles.
In (a) the matching simulated diffraction pattern for the phase $GaPd_2$ is overlaid on the left of the local FT taken from the area indicated.
The inset in (b) is the diffractogram for the entire image.

3.2. HAADF-STEM tomography

Figure 3a shows a typical image from the tilt-series, where it can be seen that the cluster analysed contains significant numbers of both small (<10 nm) and large (~20 nm) particles. A central 2D slice from the tomogram (figure 3b) displays this varied size distribution with greater clarity, and reveals a diverse range of particle morphologies. Some particles show indications of faceting, but the majority appear to be rounded and irregular in shape.

The variation in size and shape and the dense packing of the particles, as well as the noise in the tomogram, prevents immediate thresholding and binarisation to enable quantification. These factors

also mean that manual segmentation would be highly subjective and prohibitively time consuming. A semi-automated segmentation routine was therefore developed, which consisted of the following steps. A Difference of Gaussians (DoG) operation was first applied in the *x*-*y* planes of the tomogram to highlight the large particle boundaries as well as the smaller particles. The DoG filtered and original tomograms were then averaged to yield both enhanced boundaries and uniform intensity in the interiors of the particles, facilitating thresholding where the individual binarised particles could be more readily distinguished. A 3D watershed transform was then applied to separate particles that were incorrectly joined after thresholding, acting on the contrast inverted Euclidean distance map (EDM) of the binary tomogram. The severity of the watershed separation was tuned by a controlled degree of merging of the intensity minima of the contrast inverted EDM.

Figure 3c shows voxel projections of the segmented tomogram, where individual particles have been assigned a colour that differs from those of their nearest neighbours, confirming that the 3D structure of many of the larger and smaller particles has been successfully captured by the segmentation routine. Visualization in this way was used to judge the appropriate settings of the watershed transform, identifying over- and under-segmented particles.

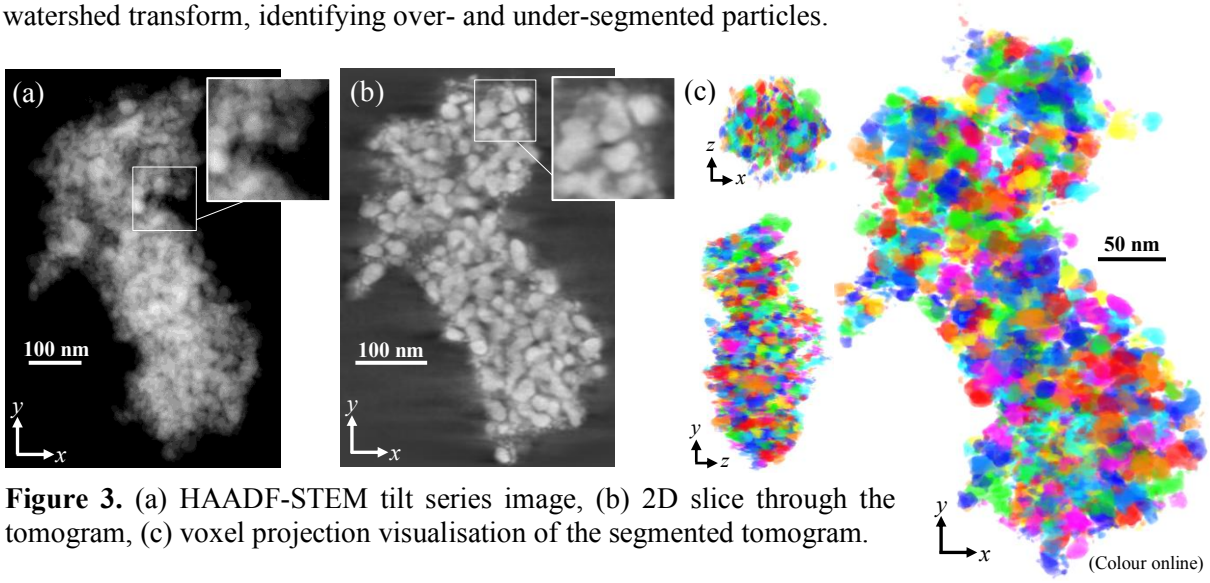

Figure 3. (a) HAADF-STEM tilt series image, (b) 2D slice through the tomogram, (c) voxel projection visualisation of the segmented tomogram.

A variety of catalytically relevant properties can be readily determined from the segmented data. Two examples are briefly presented here. The particle sizes can be gauged by considering their equivalent diameter, *d*, defined as the diameter of a sphere having the same volume as the particle. A useful indicator of the particle shape is their 3D Feret ratio (FR), defined as the maximum divided by the minimum Feret diameter. The statistical distributions of these measures are shown in figure 4.

Further insight into the size, shape and spatial distribution of the particles, and assessment of the fidelity of the segmentation and quantitative analyses, is aided by filtering of the tomogram based on the obtained measures. In figure 4a the tomogram has been split according to particle sizes, showing that particles in each size range are relatively uniformly distributed throughout the cluster. From careful inspection of each size-filtered tomogram, the particles predominantly making up each of the classes indicated in figures 4a(i)-(v) can be described as: (i) fine particles, (ii) small particles, (iii) medium particles and agglomerates of small particles, (iv) large particles and medium sized agglomerates, and (v) large agglomerates. The presence of agglomerated particles in the segmented tomogram reflects true agglomeration visible in the unprocessed data, which may be contributed to by the (suspected) remnant organic layer (cf. figure 2). However, some degree of false agglomeration may have been introduced into the tomogram by elongation effects and blurring of particle boundaries caused by the limited angular sampling of Fourier space in the original tilt-series (the so-called 'missing wedge' of unsampled information), as well as under-segmentation during the binarisation or watershed transform.

The distribution of FRs (figure 4b) suggests that the majority of particles and agglomerates are mildly anisotropic in their overall shape. Filtered tomograms showing particles with FRs lying in different ranges are shown in figures 4b(i)-(iii). This analysis will be affected to some degree by the false elongation (by a factor of ~1.2) in the missing wedge (z) direction. In particular, it is visible from figure 4b that the measured distribution is extended to the right of the mean, and the filtered tomogram for FR > 3 (figure 4b(iii)) shows that the highly anisotropic particles are mostly of the small to fine size range. Viewing this filtered tomogram in the x-z plane (not shown here) reveals that many of these particles are actually agglomerates of small/fine particles that are likely to have been falsely merged by missing wedge artefacts, as their longest dimension is almost exclusively in the z-direction.

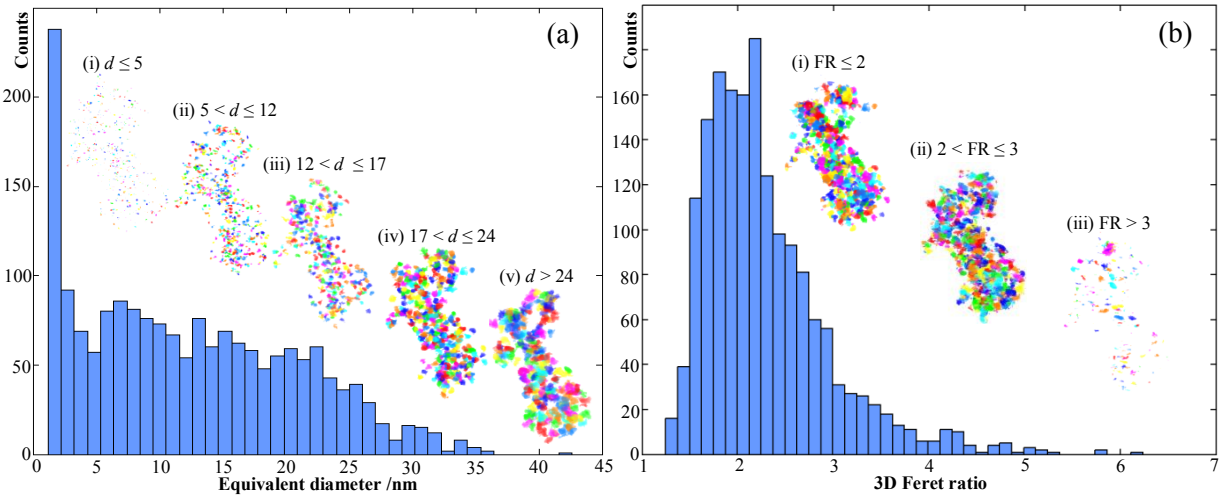

Figure 4. Statistical distributions and size/shape filtered tomograms for (a) equivalent diameter and (b) FR of the particles, based on the segmented data. (Colour online)

Overall, it is clear that the quality of the analysis is limited primarily by artefacts related to the missing wedge. Methods that overcome or negate the effects of limited angular sampling may provide the only routes to truly quantitative electron tomography. Given that the tilt range often cannot be extended for reasons of sample or hardware constraints, advanced reconstruction techniques take on particular importance. In this case, since the material of interest is known to be of single phase, improved reconstruction may be achievable using discrete algorithms [5]. Alternatively, we have recently demonstrated a new approach to reconstruction in electron tomography, known as 'compressed sensing,' which uses the prior knowledge that the object can be represented sparsely in some transform domain [6]. For samples of homogeneous composition we used the total variation transform and enforcement of sparsity in the gradient domain to produce high fidelity reconstructions, even from substantially reduced numbers of projections. Future work will involve the development of these methods, which may be applicable to samples of the type investigated here.

Acknowledgements
This work was funded by the EPSRC and the European Union under the Framework 6 program for an Integrated Infrastructure Initiative, Reference 026019 ESTEEM.

References
[1] Armbrüster M, *et al.* 2010 *J. Am. Chem. Soc.***132** 14745-47
[2] Okamoto H 2008 *J. Phase Equilib. Diff.* **29** 466-7
[3] Kovnir K, *et al.* 2008 *Z. Kristallogr.* **223** 7-8
[4] Armbrüster M, *et al.* 2011 *J. Am. Chem. Soc.* **133**, 9112-18
[5] Batenburg K J, *et al.* 2009 *Ultramicroscopy* **109** 730-40
[6] Saghi Z, *et al.* 2011 *Submitted*.